Article citation info:
Luo X, Ning J, Wu M. Design and analysis of wind turbine fault diagnosis system based on convolutional neural network. Diagnostyka. 2025;26(1):2025113. https://doi.org/10.29354/diag/201334.

DIAGNOSTYKA, 2025, Vol. 26, No. 1

e-ISSN 2449-5220
DOI: 10.29354/diag/201334

DESIGN AND ANALYSIS OF WIND TURBINE FAULT DIAGNOSIS SYSTEM BASED ON CONVOLUTIONAL NEURAL NETWORK

Xiaoli LUO [1,*], Jinye NING [2,3], Min WU [1]

[1] Scientific Research Department, Hunan Electrical College of Technology, Xiangtan, 411101, China
[2] Institute of Big Data and Artificial Intelligence Application Technology, Hunan Electrical College of Technology, Xiangtan, 411101, China
[3] School of Mechanical Engineering, Hunan University of Science and Technology, Xiangtan City, 411201, China
[*] Corresponding author, e-mail: 17369221972@163.com

Abstract

Wind turbines are apt to diverse faults during long-term operation in natural environments, which affect their power generation efficiency and lifespan. Therefore, based on convolutional neural networks, gradient descent method was introduced to optimize their parameter training. Meanwhile, synchronous compressed wavelet transform was utilized to enhance the fault signal's time-frequency information. The fault detection correlation operation was optimized through Pearson correlation coefficient. Finally, a new type of fan fault detection model was proposed. The average fault detecting accuracy of this model was the highest at 98.98%, the average loss value was the lowest at 0.08%, and the average time consumption was the shortest at 16.52s. The minimum mean square error for detecting inner and outer ring pitting of fan bearings was 0.016 and 0.018, respectively. As a result, the proposed new model performs excellently in terms of accuracy and reliability in fault detection, with detection accuracy generally superior to other existing models. This model can significantly improve wind turbine fault detection, reduce false alarm and false alarm rates, and provide effective guarantees for wind turbines' stable operation.

Keywords: convolutional neural network, wind turbines, fault, bearings, synchrosqueezed wavelet transform

1. INTRODUCTION

The global energy demand's continuous growth and environmental protection awareness's enhancement have made wind turbines a key equipment for converting wind energy into electricity. The reliability and safety of their operation are worthwhile for wind farms' stable operation [1-2]. However, due to long-term operation in complex natural environments, wind turbines are susceptible to various external factors, leading to frequent component failures. This not only increases maintenance costs, but also seriously affects wind turbines' power generation efficiency [3-4]. In recent years, many researchers both domestically and internationally have explored this issue. Cui et al. attempted to develop a new system for real-time detection of turbine faults in wind turbines. After combining Reliawind classification method and recurrent neural network, the team proposed a threshold control time detection method. This method effectively detected the operational risks of wind turbine operation and reduce false alarms [5]. After combining the thinking methods of virtual synchronization and power synchronization, Arasteh et al. proposed a new wind turbine fault detection model to improve the efficiency of unit fault detection under different wind power grid connection conditions. This method performed better than traditional models in performance evaluation during three-phase symmetrical faults [6]. Wu and Ma found that with the increasing installation of onshore and offshore wind turbines, achieving effective state monitoring became increasingly important. To this end, the team proposed a new data-driven wind turbine fault detection model by combining long short-term memory networks and other tools. This model performed more effective detection on turbines, with an accuracy of up to 94% [7].

In addition, with the developing artificial intelligence techniques, Convolutional Neural Network (CNN), as a powerful deep learning model, has obvious results in fields such as image and speech recognition. Applying CNN to wind turbine fault diagnosis can automatically extract fault

Received 2024-06-28; Accepted 2025-02-11; Available online 2025-02-18

features and improve diagnosing accuracy and efficiency by analyzing a large amount of historical and real-time monitoring data. After combining time series analysis and CNN, Rahimilarki et al. put forward a novel fault detection and classification means for wind turbines to enhance the existing technology of wind turbine fault detection and classification. This method had a high efficiency in fault detection of onshore and offshore wind turbines, with a detection error of less than 2.3% [8]. Xu et al. put forward a weighted multi-voting fault diagnosing model after incorporating multi-scale CNN and other methods to address the insufficient accuracy of intelligent models for diagnosing actual fan bearing faults. The average F1 score of this model was 97.12%, which was higher than the existing advanced methods [9]. Guo et al. found that with the developing smart grids, wind power's capacity connected to the grid gradually enhanced, making wind turbines' stable operation extremely challenging. Therefore, the team proposed a parallel multi-task fault diagnosis method after combining CNN. Compared with existing methods, the proposed method enhanced diagnostic accuracy by about 20% and had higher detection stability [10].

In summary, traditional fault diagnosing methods lean upon experience and rule libraries, which not only have low efficiency but also have strong subjectivity and high misdiagnosis rates. In recent years, many researchers have also proposed wind turbine fault detection methods using recursive neural networks and other theories, while fully utilizing CNN and its modified algorithms for wind turbine fault detection. These methods can to some extent solve wind turbines' fault detection. However, due to the variety of fault types, detection is greatly affected by environmental and other factors, resulting in a need for improvement in detection efficiency. Therefore, this study innovatively introduces Synchrosqueezed Wavelet Transform (SWT) to optimize fault signals. The clarity and resolution of signal features are improved through time-frequency domain reconstruction and compression. Pearson Correlation Coefficient (PCC) is used to enhance the correlation judgment of signal features, further optimizing fault detection performance and reducing false positives and false negatives. This research contributes to further improving fault detecting accuracy, reducing reliance on expert experience, lowering maintenance costs, and extending equipment's serving life. This research aims to provide new technical support for wind turbines' intelligent operation and maintenance.

2. METHODS AND MATERIALS

Firstly, a fault detection model for fan bearings is constructed using basic CNN. This can enable CNN to automatically extract fault features from component operation monitoring data and automatically diagnose component faults based on the extracted fault features. After completion, the study optimizes the feature signal time domain using SWT to address the insufficient sample data of wind turbine faults. Finally, a new improved CNN fan bearing fault detection model is proposed.

2.1. Wind turbines' fault detection based on convolutional neural networks

As an important renewable energy equipment, wind turbines have been widely used worldwide. As a key component of wind turbines, the operation status of bearings is directly related to the entire wind turbines' normal operation and service life [11-12]. Bearing failure not only leads to equipment shutdown, increases maintenance costs, but may also cause serious safety accidents, causing huge economic losses to wind farms. Therefore, the study introduced CNN, a deep learning detection network. It is a type of feedforward neural network that includes convolutional computation with a deep structure. It can extract sensitive feature information and input it into a classifier for diagnosis and achieve different data preprocessing [13]. The entire CNN consists of three layers. Figure 1 is a schematic diagram of convolution and pooling operations.

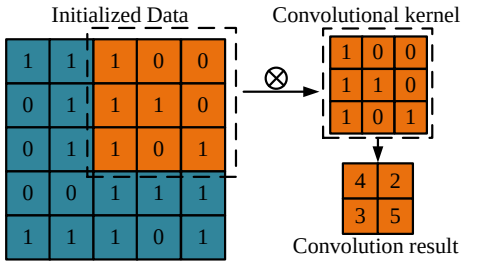

(a) Convolution operation

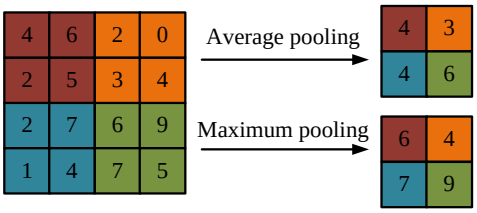

(b) Pooling operation

Fig. 1. Schematic diagram of CNN convolution and pooling operations

Figure 1 (a) shows the convolution operation. Figure 1 (b) presents the pooling operation. The convolutional layer applies multiple convolutional kernels, namely filters, to locally perceive and extract features from these input data. The pooling layer reduces data dimensionality and computational complexity through down sampling, while preserving the main features [14]. The fully connected layer classifies or regresses the extracted features. By stacking several convolutional and pooling layers, CNN can gradually learn advanced features of the data and complete target recognition

and detection. The convolution operation is represented by equation (1).

$$C_{cn} = f(X * W_{cn} + b_{cn}) \quad (1)$$

In equation (1), f means a convolutional layer activation function. X refers to the input data. W_{cn} refers to the convolutional kernel's weight. b_{cn} refers to the convolutional kernel's bias. The calculation of pooling operation is represented by equation (2).

$$a = \begin{bmatrix} 2 & 3 & 0 & 3 \\ 1 & 4 & 4 & 3 \\ 5 & 6 & 4 & 3 \\ 1 & 0 & 0 & 1 \end{bmatrix}$$
$$a \begin{bmatrix} 4 & 4 \\ 6 & 4 \end{bmatrix}_{ave} \begin{bmatrix} 2.5 & 2.25 \\ 3 & 2 \end{bmatrix}_{max} \quad (2)$$

In equation (2), a_{max} represents the maximum pooling value, which means dividing the listed numbers in a into four equal parts: top, bottom, left, right, and then selecting the maximum value from each part in order to obtain a_{max}. a_{ave} represents the average pooling value, which means dividing the listed numbers in equation EE into four equal parts: top, bottom, left, right, and then taking the average value of each part to obtain a_{ave}. The calculation of the fully connected layer is represented by equation (3).

$$y = f(W \cdot x + b_c) \quad (3)$$

In equation (3), W refers to the weight matrix. x refers to an input value. b_c represents bias. y represents output. $f(\_)$ represents an activation function. The most commonly used classification and diagnostic method for CNN in practical testing is to determine the occurrence of faults by monitoring residuals. The error diagnosis between the predicted and actual results is expressed as a cost function, which is Cross Entropy Loss Function (CELF), represented by equation (4).

$$H(p,q) = -\sum_x p(x)\, log\, q\,(x) \quad (4)$$

In equation (4), $H(p,q)$ refers to the difference between the probabilities of p and q. $p(x)$ refers to the target distribution. $q(x)$ refers to the predicted distribution. CELF is a relatively complex function and also a multivariate function. $p(x)$ and $q(x)$ are both multiple variables. Additionally, the key to optimizing CNN parameters lies in optimizing the function between each neuron node receiving or outputting to the next node, which is called the activation function. The usually optimal method is Gradient Descent (GD) [15]. This time, the objective function is defined as $A(\omega)$ to find the global minimum value, which can be represented in Figure 2.

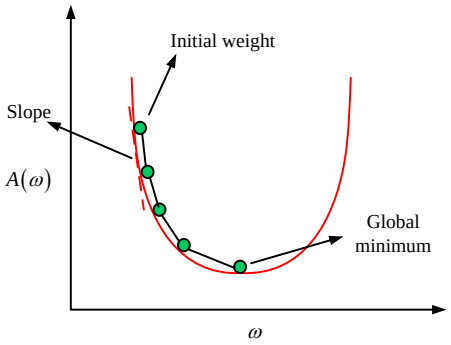

Fig. 2. Gradient descent method

In Figure 2, the quickest way to reach the global lowest point from the initial weight position is to take the partial derivative of the steepest point, which is called gradient. By taking partial derivatives multiple times, when a minimum $A(\omega)$ is reached, an optimal solution can be obtained. In summary, a wind turbine bearing fault diagnosing model is constructed by combining CNN in Figure 3.

In Figure 3, the entire fault detection model can be divided into data preprocessing and CNN detection modules. Among the data preprocessing is to take the input data as the time series vibration signals of the wind turbine operation state, after preprocessing, the input matrix size is 128x128, where the rows represent the time series and the columns represent the eigenfrequencies collected by different sensors. The data is normalized to ensure that the input data eigenvalues are between 0 and 1, which reduces the interference of outliers on the model. After three preprocessing steps, namely

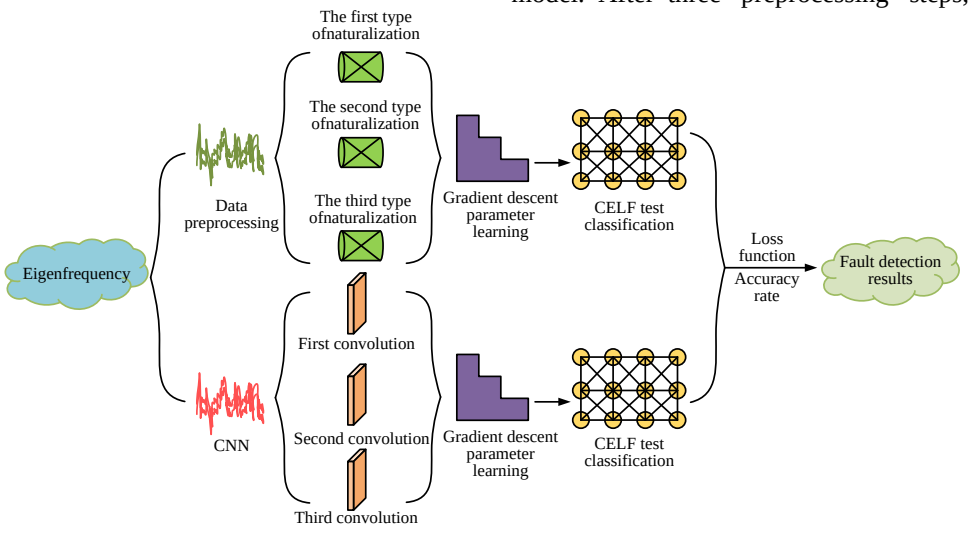

Fig. 3. CNN wind turbine bearing fault detection model

cleaning, conversion, and integration, GD performs parameter learning. After completion, wind turbine fault classification is achieved through CELF. On the other hand, the characteristic frequency data of the initial fan operation are inputted and processed by a three-layer convolutional network for data convolution, pooling, and other operations. After completion, GD also performs parameter learning. Finally, wind turbine fault classification is uniformly achieved through CELF. The classification results of two fault detections are output. The authenticity is judged based on the loss function and accuracy to determine the best detection result.

2.2. Optimization of fault diagnosis models for large amounts of fault feature data

The above content has completed the construction of a basic CNN fan fault detection model. In wind turbines' operation, there used to be very limited real data available for model training, which resulted in low diagnostic accuracy [16-17]. Therefore, the study first analyzes the failure mechanism and characteristics of mechanical components in wind turbines' transmission system. Figure 4 is the on-site diagram and structural schematic diagram of wind turbines' bearing components.

a) On-the-spot picture

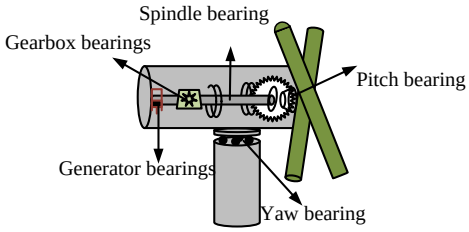

b) Simplified schematic structure

Fig. 4. On-site diagram and structural schematic diagram of wind turbine bearing components

Figure 4 (a) shows the on-site view of wind turbines' bearing components. Figure 4 (b) shows the structure of wind turbines' bearing components. These bearing components are divided into spindle, generator, pitch, yaw, and gearbox bearings [18]. The main shaft bearing is the most critical, responsible for the load-bearing of the hub and blades. The influencing factors during operation are more complex, making it difficult to replace the damaged bearing. In the failure or damage, the periodic operation data of bearings are generally collected by multiple sensors. The study installed four high-precision vibration sensors at key components of the wind turbine, which were installed at the main shaft bearing, generator bearing, gear box and yaw bearing. These locations are able to effectively collect the mechanical vibration signals generated by the WTGs during operation, ensuring comprehensive coverage of fault characteristics. The general spindle bearing faults are divided into inner and outer rings, rolling element, and cage faults [19]. The characteristic frequencies of various types of faults are represented by equation (5).

$$\begin{cases} f_1 = \frac{N}{2}(1+\frac{d_b}{D}cos\,\alpha)f_r \\ f_2 = \frac{N}{2}(1+\frac{d_b}{D}cos\,\alpha)f_r \\ f_3 = \frac{D}{d_b}(1-\frac{d_b}{D}cos\,\alpha)^2 f_r \\ f_4 = \frac{1}{2}(1-\frac{d_b}{D}cos\,\alpha)f_r \end{cases} \tag{5}$$

In equation (5), f_1, f_2, f_3, and f_4 refer to inner ring, outer ring, rolling element, and cage faults' characteristic frequencies, respectively. N and d_b refer to the quantity and diameter of rolling elements, respectively. α represents a contact angle. D refers to the bearing diameter. f_r represents the bearing rotation frequency. Due to the various load factors of the spindle bearings, there is also signal interference during operation. Simple directional detection cannot meet the requirements. In addition, after a sudden failure, the natural vibration frequency of the bearing will be affected by impact pulses, such as inner and outer rings' frequency suddenly changing from thousands of hertz to tens of thousands of hertz. The inner and outer rings' frequency variation is represented by equation (6).

$$f_n = \frac{n(n^2-1)}{2\pi(\frac{D}{2})^2\sqrt{n^2+1}}\sqrt{\frac{EI}{M}} \tag{6}$$

In equation (6), E represents the material's elastic modulus. M refers to the mass per unit length. I refers to the cross-section's inertia of the ring. n refer to the vibration order. If the spindle bearing uses steel balls, its natural frequency is represented by equation (7).

$$f_{bn} = \frac{0.848}{d}\sqrt{\frac{EI}{2\rho}} \tag{7}$$

In equation (7), d represents the steel ball's diameter. ρ represents its density. If a local fault occurs suddenly, the frequency measured by the sensor at the main shaft bearing will change from sinusoidal vibration to a short-term, frequency increasing vibration. However, if there are multiple faults, the characteristic frequencies will superimpose, causing a single vibration signal to weaken. Therefore, SWT is introduced to enhance the density and energy of the original signal characteristic frequencies. This method was proposed by Daubechies et al. in 2011 [20]. The main idea is to redistribute the coefficients of wavelet transform to the estimated instantaneous frequency, usually manifested as the derivative of time. Figure 5 shows the transformation method of SWT.

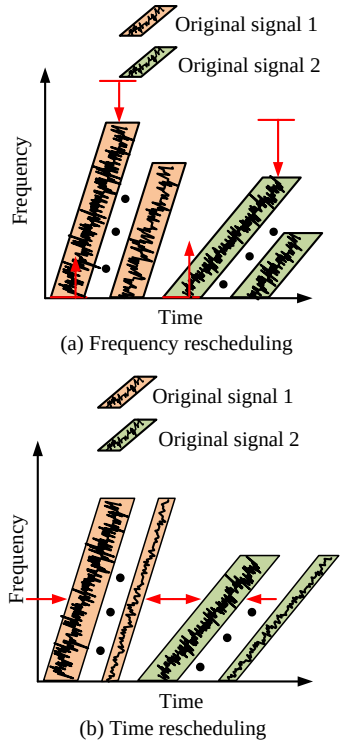

Fig. 5. The transformation principle of SWT

Figure 5 (a) shows the synchronous compression transformation of SWT signals based on frequency. Figure 5 (b) shows the synchronous compression transformation of SWT signals over time. Where the brown pattern is the original time-frequency signal and the green pattern is the time-frequency of the signal after SWT transformation. Each synchronous compression method can sharpen the time-frequency representation and maintain the signal energy state. This makes the frequency components of the signal independent of each other, without the phenomenon of frequency modulation or divergence. The vibration signal's continuous wavelet transforming of wind turbine rolling bearings is represented by equation (8).

$$W_x(a,b;\psi) = \int x(t) a^{-1/2} \psi(\frac{t-b}{a}) dt \quad (8)$$

In equation (8), $W_x(a,b;\psi)$ represents signal $x(t)$'s wavelet system spectrum. ψ represents a mother wavelet function. $a^{-1/2}$ represents the standardized constant. a and b refer to scale and time shift factors. At this point, the calculation of SWT is represented by equation (9).

$$T_x(\omega_l, b) = \frac{1}{\Delta\omega} \sum_{z_k | \omega_x(a,b) - \omega_l | \le \frac{\Delta\omega}{2}} W_x(a,b;\psi) z_k \quad (9)$$

In equation (9), ω_l represents a specific frequency. z_k represents discrete scale. k represents the quantity of scales. The discretization of frequency and scale is represented by equation (10).

$$\begin{cases} \Delta\omega = \omega_l - \Delta\omega_{l-1} \\ \Delta z_k = z_k - \Delta z_{k-1} \end{cases} \quad (10)$$

After discretization is completed, the time-domain reconstruction of the feature signal can be performed through the SWT of reversible transformation. The reversible transformation is represented by equation (11).

$$\begin{cases} f(t) = 2\,Re[\frac{1}{C_\phi} \sum_l T_x(\omega_l, b) \Delta\omega] \\ C_\phi = \int_0^\infty \frac{\psi^*(\xi)}{\xi} d\xi \end{cases} \quad (11)$$

In equation (11), C_ϕ represents a finite value. $\psi^*(\xi)$ represents the conjugate Fourier transform of wavelet functions. After continuous wavelet transform of the signal, SWT compresses and rearranges the wavelet coefficients in the time-frequency domain, resulting in a clearer time-frequency expression of the signal. In addition, PCC was introduced to distinguish between two signals more clearly and avoid overlap. Two signals' PCC is represented by equation (12).

$$corr\_coef = \frac{\sum_{i=1}^n (x_{pi} - \bar{x}_p)(y_{pi} - \bar{y}_p)}{\sqrt{\sum_{i=1}^n (x_{pi} - \bar{x}_p)^2} \sqrt{\sum_{i=1}^n (y_{pi} - \bar{y}_p)^2}} \quad (12)$$

In equation (12), x_{pi} and $\bar{x}_p$ represent the data point and mean value of vector x_p, respectively. y_{pi} and $\bar{y}_p$ represent the data point and mean value of vector y_p. In summary, based on the previously proposed CNN wind turbine bearing fault detection model, a new intelligent fault diagnosing structure is finally put forward combined with SWT signal data optimization and PCC correlation judgment for wind turbines. Figure 6 shows the model process.

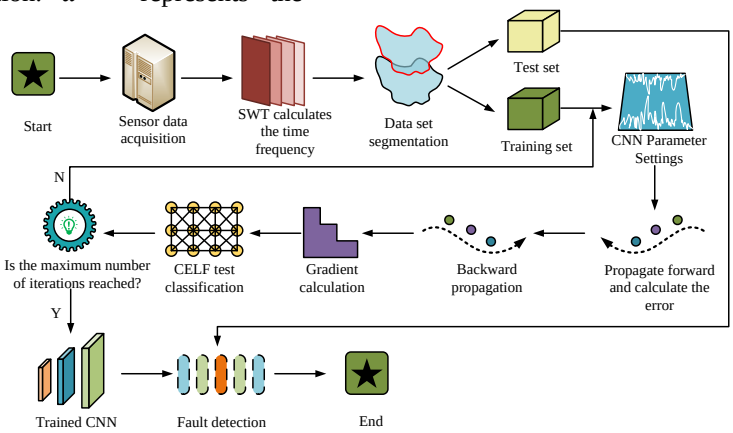

Fig. 6. Process of intelligent fault diagnosis model for new wind turbines

In Figure 6, firstly, vibration signals are collected by sensors installed at various locations of the wind turbine. Time-frequency distribution is calculated by SWT to divide the dataset, which can be separated into training and testing sets. Next, some signal data from a training set are used as input to set CNN parameters and initialize this network. For example, the convolutional layer uses convolutional kernels of size 3×3, with a total of 64 convolutional kernels set for extracting local features; the pooling layer uses maximum pooling with pooling kernels of size 2×2. ReLU is used as an activation function after each convolutional layer, which helps the network to introduce nonlinear features. The CNN model contains a total of three convolutional layers and two pooling layers, and finally, fault classification is performed by a fully connected layer. The architecture of the entire CNN model is an input layer, 3 convolutional layers, 2 pooling layers, and a fully connected layer with a total depth of 6 layers. Then, the training set propagates forward to calculate the error, uses GD to update the parameters, and then backpropagates until the error is calculated. During the process, fault classification is achieved using CELF. If the training reaches the maximum round at this time, the trained CNN is exported. Finally, fault diagnosis is performed on the input test set. If the training does not reach the maximum round, the CNN parameter initialization is returned.

3. RESULTS

Firstly, an experimental environment was established to verify the intelligent fault diagnosis model of this new wind turbine. The model parameters were set and ablation, loss function, and multi-indicator tests were conducted. In addition, these three types of fault classification detection performance of this new model was tested on a real wind turbine operation test bench and evaluated using error indicators.

3.1. Performance testing of intelligent fault diagnosis model for new wind turbines

A suitable experimental platform was established to verify the newly proposed intelligent fault diagnosis model for wind turbines. The CPU is Intel Core i7-9700. The GPU is NVIDIA GeForce RTX 1660s. The operating system adopts Windows 10, 64 bit. The convolutional layer has a step size of 16, the pooling layer has a step size of 2, the optimizer uses Adam, the batch is 128, and the iteration is 15. The data sampling frequency is 53000Hz, the motor's rated speed is 1520r/min, and the power frequency is 80Hz. Each type of fault data has a sample size of 12 and a sample length of 1 second. A total of 500 data after 40 min of sampling are divided into training and test sets in the ratio of 8:2. During the model training process, the training set is used for the optimization of model parameters, the validation set is used for the tuning of hyper-parameters, and the test set is used for the final evaluation of model performance. In this case, the ablation test assesses the relative importance of each module by gradually removing key components of the model, such as the simultaneous compressed wavelet transform, Pearson's correlation coefficient, and gradient descent method, and observing the change in the model performance. The final improved CNN fault detection model was validated through ablation testing with detection accuracy as the indicator in Figure 7.

Figure 7 (a) shows the improved model's ablation test results in the training set. Figure 7 (b) presents the improved model's ablation test results in the test set. For stability, after combining GD, SWT, and PCC, the improved CNN fan bearing fault detection was stable at around 99%. According to the test set

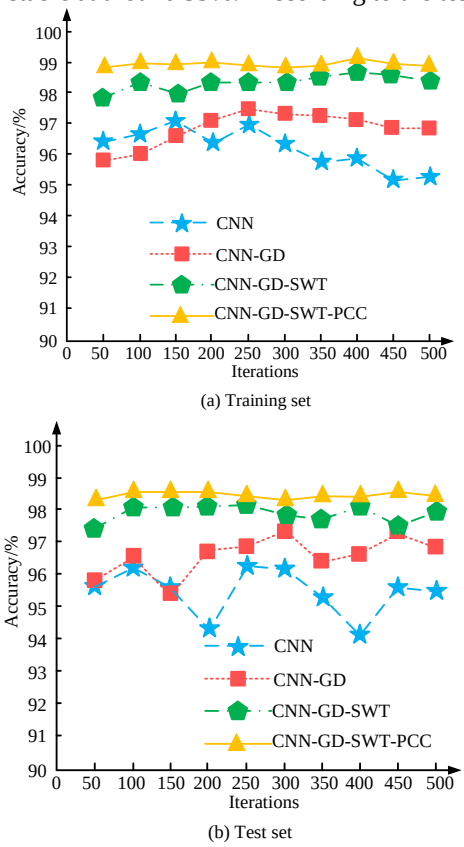

(a) Training set

(b) Test set

Fig. 7. The ablation test results of improved CNN fault detection model

data, the average accuracy of fault monitoring for individual CNN modules was about 96%. After GD, SWT, and PCC optimization, the overall model's fault detection accuracy increased to 98.5%. This indicated that each module positively promoted the overall model functionality. In addition, the study took the loss function as the testing indicator and introduced popular fault detection models for wind turbines of the same type. The loss function is one of the key metrics for model optimization, which measures the gap between the model's predicted results and the actual labels. They include Support Vector Machine-based Wind Turbine Fault Detection Model (SVM-WTFD), Random Forest-

based Wind Turbine Fault Detection Model (RF-WTFD), Autoencoder-based Wind Turbine Fault Detection Model (AE-WYFD), and Long Short-Term Memory Network-based Wind Turbine Fault Prediction Model (LSTM-WTFP). Figure 8 shows the test results.

Figure 8 (a) presents SVM-WTFD and the proposed model's loss functions. Figure 8 (b) presents RF-WTFD and the proposed model's loss functions. Figure 8 (c) presents AE-WTFD and the proposed model's loss functions. Figure 8 (d) presents LSTM-WTFD and the proposed model's loss functions. In the comparison of four fan fault detection models, they all had similar loss function values to the proposed model in the later stage. The loss function can reflect a model's detecting quality.

If the value is small, the fault detection accuracy is high. By comparison, the other three models' loss function values in the early stage were all 14. The proposed model had the highest value of only 8, which tended to 5 after stable operation in the later stage. The above models were continued to be tested using average accuracy, average loss, average time consumed, precision (Precision), recall (Recall) and F1 value as metrics. Among them, the average accuracy rate indicates the proportion of the model correctly classified in all the test samples, which is the basic index to measure the overall classification ability of the model; the average loss is used to evaluate the prediction error of the model. The smaller the value of the loss function, the closer the model's prediction results are to the true value; the F1 value is the reconciled average of the precision rate and the recall rate, which provides a balanced evaluation of them, and is particularly suitable for use in the case of imbalance between positive and negative class samples, and is used to comprehensively evaluate the model's classification performance. The test results are shown in Table 1.

In Table 1, SVM-WTFD and LSTM-WTF performed average in two types of real wind turbine fault datasets. The accuracy, loss values, and running time between these two models and the proposed model had obvious differences. RF-WTFD and AE-WTFD effectively improved the detection effectiveness through their respective optimization methods. The highest average detection accuracy was 95.27% and 95.83%, respectively. The lowest average loss values were 0.19% and 0.16%, respectively. The shortest average time consumption was 43.21s and 27.63s, respectively. The proposed model's average detecting accuracy was the upmost at 98.98%, the average loss value was the lowest at 0.08%, and the average time consumption was the shortest at 16.52s. In addition, the comprehensive performance advantages of the proposed model are further demonstrated by introducing new evaluation metrics such as precision rate, recall rate and F1 score. In comparison with other models, the proposed model also performs well in terms of precision rate and recall, reaching 97.12% and 97.03% precision rate and 98.01% and 97.85% recall

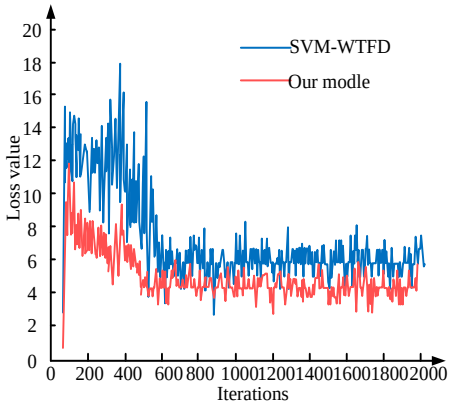

(a) SVM-WTFD

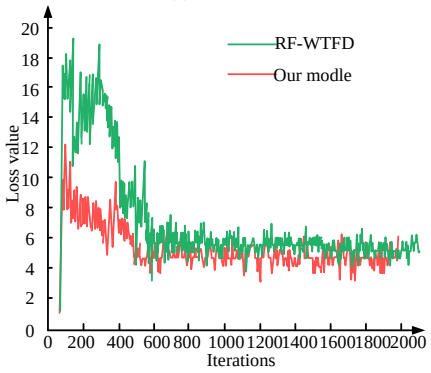

(b) RF-WTFD

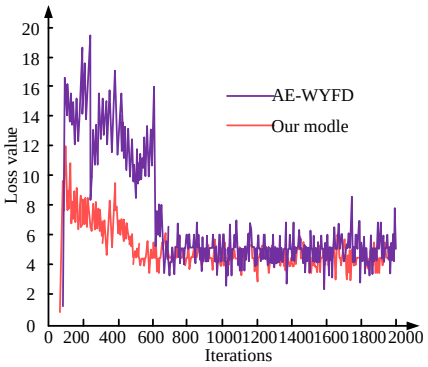

(c) AE-WYFD

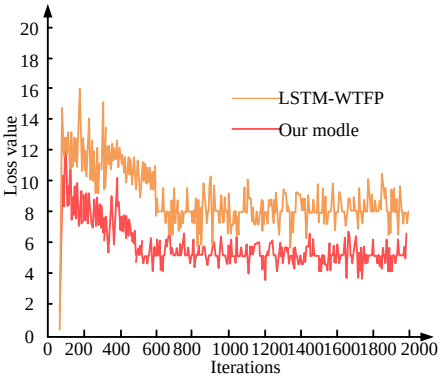

(d) LSTM-WTFP

Fig. 8. Test results of loss functions for different models

rate on the two datasets, which are higher than the comparison models such as SVM-WTFD and RF-WTFD. This indicates that the model is more effective in identifying the actual faults in the

detected fault samples and reduces the false alarms. In summary, the proposed new fan bearing fault detection model had certain reliability and effectiveness, whose detection performance was obvious in existing methods.

3.2. Simulation testing of intelligent fault diagnosis model for new wind turbines

The study conducted simulation tests on the motor bearing operation database of Case Western Reserve University to validate the ew fan bearing fault detection model's practical application effect. The motor power used in this motor test bench was 1521W, and the sampling frequency was set to two types: 12kHz and 48kHz. The output position of the motor adopted a pair of torque sensors to collect the output data and monitor the real-time operation status of the motor under different scenes. The fault implantation method adopted single point damage of electrical discharge machining. The complexity of the implanted fault varied and was located at different positions of the motor bearing. General motor bearing faults can be divided into three types: inner and outer rings and rolling element faults. During the construction of the dataset, the study collected operational data for both healthy and faulty bearings. The faulty bearing data includes inner ring pitting, outer ring pitting and rolling element failure, and the faulty bearing accounts for 60% of the total data, while the proportion of healthy bearings is 40%. Such data distribution can be closer to the actual wind turbine operation state, and it helps to improve the model's sensitivity to fault conditions and enhance its generalization ability in detecting faults. Table 2 shows the specific experimental motor parameters.

In Table 2, under the same data collection location, collection frequency, and motor bearing speed conditions, different types of faults were generated, resulting in different fault diameters. However, as the bearing speed increased, the fault diameter became larger. In addition, under the same collection location, sampling frequency, and speed, the fault diameter of rolling element pitting was significantly larger than that of inner and outer ring pitting. The research focused on non-pitting, rolling element pitting, and inner and outer ring pitting as the testing backgrounds. Popular fault detection models of the same type were introduced, such as Transfer Learning (TL), Current Monitoring (CM), and Time Domain (TD). Figure 9 shows the classification detection results of faults.

Table 1. Test results of indicators for different models

Data set	Model	Average accuracy/%	Average loss/%	Average elapsed time/s	Precision/%	Recall/%	F1 score/%
NREL Wind Data	SVM-WTFD	94.67	0.34	55.76	91.52	92.11	91.81
	RF-WTFD	93.21	0.27	51.54	90.12	91.34	90.72
	AE-WTFD	95.83	0.29	38.63	93.75	94.02	93.88
	LSTM-WTFD	91.74	0.16	31.57	89.52	89.64	89.58
	Our model	98.98	0.09	16.52	97.12	98.01	97.56
CWS	SVM-WTFD	96.84	0.27	59.67	94.21	94.95	94.58
	RF-WTFD	95.27	0.19	43.21	92.48	93.12	92.83
	AE-WTFD	93.22	0.16	28.79	91.58	91.67	91.62
	LSTM-WTFD	94.68	0.22	27.63	92.35	92.98	92.66
	Our model	98.93	0.08	18.21	97.03	97.85	97.44

Table 2. Motor operating parameters table

Collection location	Speed (r/min)	Fault type	Fault diameter/mm	Sampling frequency/kHz
Driving end	1530, 1550, 1572	No	No	48
Driving end	1530	Outer ring pitting	0.177	48
Driving end	1550	Outer ring pitting	0.356	48
Driving end	1572	Outer ring pitting	0.524	48
Driving end	1530	Inner ring pitting	0.179	48
Driving end	1550	Inner ring pitting	0.367	48
Driving end	1572	Inner ring pitting	0.571	48
Driving end	1530	Rolling body pitting	0.167	48
Driving end	1550	Rolling body pitting	0.352	48
Driving end	1572	Rolling body pitting	0.602	48

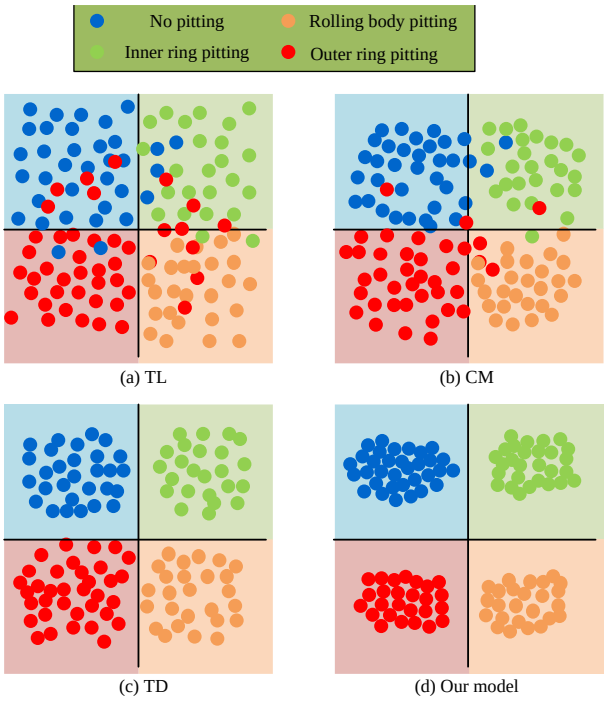

Fig. 9. Fault classification detection results of different modelsFigure 9 (a) shows TL's fault classification detection results

Figure 9 (b) presents the fault classification detection results of CM. Figure 9 (c) presents the fault classification detection results of TD. Figure 9 (d) presents the fault classification detection results of the proposed model. From Figure 9, it can be seen that the TL model and the CM model have lower fault classification accuracy, poor overall results, and obvious generalization problems when dealing with different working conditions, such as no pitting, rolling body pitting, inner ring pitting, and outer ring pitting. In particular, under multiple fault conditions, the two models have higher false alarm and omission rates, leading to significant deviations in the fault classification results. In contrast, the TD model improves in fault detection performance, but its stability and accuracy are still far less than the proposed model. In several fault categories, the classification results of the TD model are still not precise enough, and the detection ability of some weak faults is poor. The proposed model, on the other hand, successfully improves the fault feature extraction capability by introducing SWT for time-frequency information enhancement and PCC for fault correlation calculation. The model is able to effectively screen out the fault information with weak features, thus greatly improving the accuracy of fault classification and the generalization ability of the model, especially in the performance under complex working conditions. Finally, the study compared and tested the four models using Mean Squared Error (MSE) and Mean Absolute Error (MAE) as indicators in Figure 10.

Figure 10 (a) shows the MSE test results of four models. Figure 10 (b) presents four models' MAE test results. As can be seen in Figure 10, the consistency of the detection results among all four models indicates that rolling body pitting is detected better than inner and outer ring pitting, and this trend is consistent with the numerical settings in Table 2. Specifically, all four models exhibited the lowest MSE and MAE values for rolling body pitting, followed by inner ring pitting, and the highest MSE and MAE values for outer ring pitting. Among these four models, the study of the proposed model showed the best performance in both MSE and MAE values. In particular, in the detection of rolling body pitting faults, the MSE and MAE of the proposed model are 0.013 and 0.028, respectively, which are significantly lower than the other models. The MSE and MAE values of inner ring pitting and outer ring pitting are also significantly lower than those of other models, which are 0.016 and 0.037, and 0.018 and 0.047, respectively. This indicates that the proposed model has higher accuracy and reliability in the detection of different fault types, and especially outperforms other existing fault detection models in terms of its ability to recognize for minor faults.

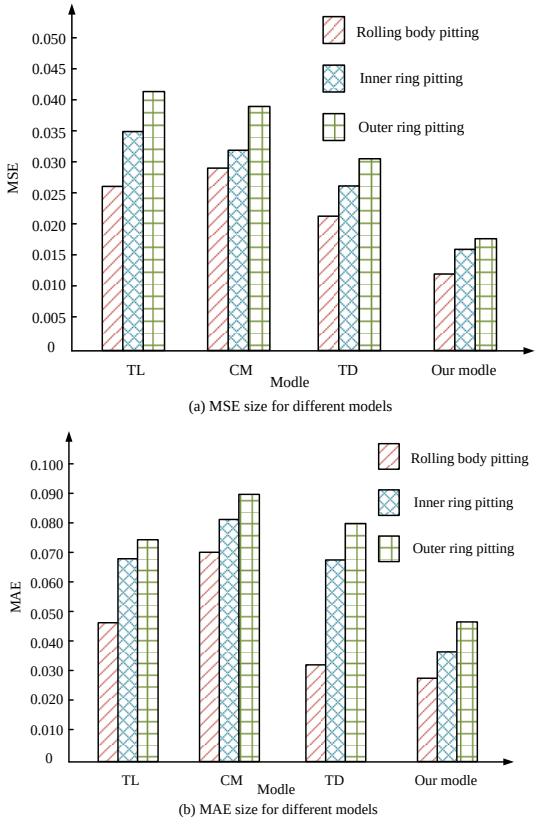

Fig. 10. MSE and MAE of different models

4. CONCLUSION

In response to frequent faults caused by wind turbines operating in complex natural environments, this study was based on CNN and introduced GD, SWT, and PCC for fault feature enhancement and classification, respectively. Finally, the detection and optimization of wind turbine fault information were realized. In a training set, the new type of fan

bearing's fault detection was stable at around 99%. In a test set, this new fan bearing fault detection model's accuracy slightly decreased to 98.5%. Compared to other similar detection models, this new model had a maximum loss function value of 8, which tended to 5 after stable operation in the later stage, and the value maximally decreased by 6. In the indicator detection, the average detection accuracy of this new model was the highest at 98.98%, the average loss value was the lowest at 0.08%, and the average time was the shortest at 16.52s. In simulation testing, the new model maintained ultra-high accuracy and stably classified and detected four working conditions: no pitting, rolling element pitting, and inner and outer ring pitting. The minimum MSE and MAE of rolling element pitting in this model were 0.013 and 0.028, respectively. The minimum MSE and MAE of inner ring pitting were 0.016 and 0.037, respectively. The minimum MSE and MAE of outer ring pitting were 0.018 and 0.047, respectively. In summary, improving the CNN wind turbine fault diagnosis model has high reliability and effectiveness in practical applications, which can significantly enhance wind turbines' operational stability and reduce maintenance costs. However, the study has not yet included more fan faults for model detection. Subsequent research can consider expanding and incorporating more real fan operation fault data to verify the effectiveness of the model.

Source of funding: *The research is supported by achievement of the 2024 Hunan Provincial Natural Science Foundation project "Intelligent Fault Diagnosis and Remaining Life Prediction of Wind Turbine Units Based on Deep Learning" (No. 2024JJ7095), as well as the 2023 Hunan Provincial Natural Science Foundation project "Key Technologies Research of Multi-source Data Fusion and Application for Intelligent Control of Wind Farms Aimed at Enhanced Absorption" (No. 2023JJ60183).*

Author contributions: *research concept and design, X.L.; Collection and/or assembly of data, J.E.; Data analysis and interpretation, X.L., M.W.; Writing the article, X.L.; Critical revision of the article, J.E., M.W.; Final approval of the article, X.L., M.W.*

Declaration of competing interest: *The authors declare that they have no known competing financial interests or personal relationships that could have appeared to influence the work reported in this paper.*

REFERENCES

1. Yi H, Jiang Q, Yan X. Imbalanced classification based on minority clustering synthetic minority oversampling technique with wind turbine fault detection application. IEEE Transactions on Industrial Informatics. 2021;17(9):5867-5875. https://doi.org/10.1109/TII.2020.3046566.
2. Liu X, Yang L, Zhang Z. Short-term multi-step ahead wind power predictions based on a novel deep convolutional recurrent network method. IEEE Transactions on Sustainable Energy. 2021;12(3):1820-1833. https://doi.org/10.1109/TSTE.2021.3067436.
3. Corley B, Koukoura S, Carroll J, McDonald A. Combination of thermal modelling and machine learning approaches for fault detection in wind turbine gearboxes. Energies. 2021;14(5):1375-1376. https://doi.org/10.3390/en14051375.
4. Badihi H, Zhang Y, Pillay P. Fault-tolerant individual pitch control for load mitigation in wind turbines with actuator faults. IEEE Transactions on Industrial Electronics. 2021;68(1):532-543. https://doi.org/10.1109/TIE.2020.2965479.
5. Cui Y, Bangalore P, Tjernberg LB. A fault detection framework using recurrent neural networks for condition monitoring of wind turbines. Wind Energy. 2021;24(11):1249-1250. https://doi.org/10.1002/we.2628.
6. Arasteh A, Zeni L, Cutululis NA. Fault ride through capability of grid forming wind turbines: A comparison of three control schemes. IET Renewable Power Generation. 2022; 16(9): 1866-1881. https://doi.org/10.1049/icp.2021.1349.
7. Wu Y, Ma X. A hybrid LSTM-KLD approach to condition monitoring of operational wind turbines. Renewable Energy. 2022; 181(1): 554-566. https://doi.org/10.1016/j.renene.2021.09.067.
8. Rahimilarki R, Gao Z, Jin N, Zhang A. Convolutional neural network fault classification based on time-series analysis for benchmark wind turbine machine. Renewable Energy. 2022; 185(2): 916-931. https://doi.org/10.1016/j.renene.2021.12.056.
9. Xu Z, Mei X, Wang X, Yue M, Jin J, Yang Y, Li C. Fault diagnosis of wind turbine bearing using a multi-scale convolutional neural network with bidirectional long short term memory and weighted majority voting for multi-sensors. Renewable Energy. 2022, 182(1): 615-626. https://doi.org/10.1016/j.renene.2021.10.024.
10. Guo S, Yang T, Hua H, Cao J. Coupling fault diagnosis of wind turbine gearbox based on multitask parallel convolutional neural networks with overall information. Renewable Energy. 2021; 178(11): 639-650. https://doi.org/10.1016/j.renene.2021.06.088.
11. Xing Z, Chen M, Cui J, Chen Z, Xu J. Detection of magnitude and position of rotor aerodynamic imbalance of wind turbines using convolutional neural network. Renewable Energy. 2022; 197(9): 1020-1033. https://doi.org/10.1016/j.renene.2022.07.152.
12. Zhang Z, Doganaksoy N. Change point detection and issue localization based on fleet-wide fault data. Journal of Quality Technology. 2022; 54(1): 453-465. https://doi.org/10.1080/00224065.2021.1937409.
13. Zheng X, Zeng Y, Zhao M, Vebkatesh B. Early identification and location of short-circuit fault in grid-connected AC microgrid. IEEE Transactions on Smart Grid. 2021;12(4):2869-2878. https://doi.org/10.1109/TSG.2021.3066803.
14. Dao PB. Condition monitoring and fault diagnosis of wind turbines based on structural break detection in SCADA data. Renewable Energy. 2022;185(3):641-654. https://doi.org/10.1016/j.renene.2021.12.051.
15. Peng Y, Qiao W, Qu L. Compressive sensing-based missing-data-tolerant fault detection for remote condition monitoring of wind turbines. IEEE Transactions on Industrial Electronics. 2021;69(2): 1937-1947. https://doi.org/10.1109/TIE.2021.3057039.
16. Wang X, Tang G, Yan X, He Y, Zhang X, Zhang C. Fault diagnosis of wind turbine bearing based on

optimized adaptive chirp mode decomposition. IEEE Sensors Journal. 2021; 21(12): 13649-13666. https://doi.org/10.1109/JSEN.2021.3071164.
17. Jin X, Nian H. Overvoltage suppression strategy for sending AC grid with high penetration of wind power in the LCC-HVdc system under commutation failure. IEEE Transactions on Power Electronics. 2021;36(9):10265-10277. https://doi.org/10.1109/TPEL.2021.3066641.
18. Wang MH, Lu SD, Hsieh CC. Fault detection of wind turbine blades using multi-channel CNN. Sustainability. 2022;14(3):1781-1783. https://doi.org/10.3390/su14031781.
19. Vives J. Vibration analysis for fault detection in wind turbines using machine learning techniques. Advances in Computational Intelligence. 2022;2(1):15-16. https://doi.org/10.1007/s43674-021-00029-1.
20. Hebbi C, Mamatha H. Comprehensive dataset building and recognition of isolated handwritten Kannada characters using machine learning models. Artificial Intelligence and Applications. 2023; 1(3): 179-190. https://doi.org/10.47852/bonviewAIA3202624.

Xiaoli Luo holds a Master's degree in Industrial Engineering from China University of Geosciences and is a Professor at Hunan Electrical College of Technology. She has served as the Dean of the Wind Energy Engineering Department and Director of the Research Office at the same institution. She has led five provincial-level projects, including those funded by the Hunan Natural Science Foundation, and has published over 40 papers. Her main research focus is on wind power fault diagnosis.
Contact: 17369221972@163.com

Jinye Ning obtained her Master's degree in Electronic Science and Technology (2009) from the University of Electronic Science and Technology of China. She is currently an Associate Professor at Hunan Electrical College of Technology and a PhD candidate at Hunan University of Science and Technology, focusing on collaborative control of offshore wind turbines. She has led six provincial-level projects and published 13 papers as the first author. She is also a Young Core Teacher of Hunan Province and serves as a member of various academic committees. Her research interests include wind turbine control and fault diagnosis.
Contact: njynjy2023@163.com

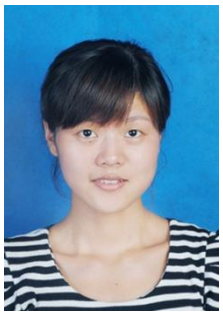

Min Wu obtained her Master's degree (2017) from Xiangtan University, Hunan, China. Presently, she is working as an Associate Professor in the Hunan Electrical College of Technology, Hunan, China. She has published more than 10 articles in reputed journals. Her research focuses on big data analysis.
Contact: dodowoo@foxmail.com